Journal of Shahrekord University of Medical Sciences
doi:10.34172/jsums.1186 2026;28(4): 199-207 http://j.skums.ac.ir

Original Article

Transcriptomic and Network Analyses Identify Cell Cycle-Associated Candidate Driver Genes and a Neuronal Gene Expression Signature in Glioblastoma

Elaheh Maherani[1], Maryam Peymani[1*], Samira Asgharzade[2*], Ali Zarrabi[3], Fatemeh Azizi Farsani[4]

[1]Department of Biology, Shk. C., Islamic Azad University, Shahrekord, Iran
[2]Cellular and Molecular Research Center, Basic Health Sciences Institute, Shahrekord University of Medical Sciences, Shahrekord, Iran
[3]Department of Biomedical Engineering, Faculty of Engineering and Natural Sciences, Istinye University, Istanbul 34396, Turkiye
[4]Medical Plants Research Center, Basic Health Sciences Institute, Shahrekord University of Medical Sciences, Shahrekord, Iran

*Corresponding Authors: Maryam Peymani, Emails: m.peymani@iau.ac.ir; Peymani62_m@yahoo.com and Samira Asgharzadeh, Email: asgharzade1396@gmail.com

Abstract

Introduction: Glioblastoma (GBM) is the most aggressive primary brain tumor, with a median survival of approximately 15 months. Its marked molecular heterogeneity contributes to treatment resistance. Accordingly, this study aimed to define the dominant transcriptional programs altered in GBM and to prioritize cell cycle-associated candidate genes for future validation.

Methods: Transcriptomic data from the Cancer Genome Atlas GBM cohort (TCGA-GBM; 156 tumor and 5 normal samples) were normalized in R, retaining 10,118 genes. Differential expression analysis, using thresholds of absolute log2 fold change ($|\log2FC| > 0.5$ and adjusted $P < 0.05$, identified 7,469 differentially expressed genes (DEGs). Then, a focused 142-gene panel was used for downstream analyses. A log2FC heatmap visualized the top 50 DEGs. Gene ontology (GO) and Kyoto Encyclopedia of Genes and Genomes (KEGG) enrichment analyses were performed, followed by a circular gene–pathway interaction network using the *circlize* package.

Results: Among DEGs, 4,789 (64.1%) were downregulated, and 2,680 (35.9%) were upregulated. The top 50 DEGs included three highly upregulated genes (*TOP2A*, *LTF*, and *IGFBP2*) and a predominantly downregulated neuronal/synaptic signature. KEGG identified the cell cycle and focal adhesion pathways as significantly enriched, while GO highlighted the mitotic cell cycle and nuclear division. Network analysis prioritized *CDC20*, *CCNA2*, *CCNB1*, *WEE1*, *MYC*, *E2F5*, and *BUB1* as key cell cycle-associated candidates.

Conclusion: GBM demonstrated extensive transcriptional dysregulation, with neuronal gene suppression and activation of proliferative programs. Overall, *CDC20*, *CCNA2*, *CCNB1*, *WEE1*, *MYC*, *E2F5*, and *BUB1* are promising candidates for future functional studies and therapeutic targeting.

Keywords: Glioblastoma, Gene expression profiling, Gene ontology, Signal transduction, Cell cycle

Received: June 26, 2026, **Revised:** August 12, 2026, **Accepted:** August 15, 2026, **ePublished:** November 19, 2026

Introduction

Glioblastoma (GBM) is considered the most aggressive primary malignancy of the central nervous system, and outcomes remain poor despite advances in surgery, radiotherapy, and chemotherapy (1, 2). According to the 2021 World Health Organization classification of central nervous system tumors, GBM is molecularly defined as an isocitrate dehydrogenase-wildtype diffuse astrocytic glioma characterized by different features; they include necrosis, microvascular proliferation, epidermal growth factor receptor amplification, telomerase reverse transcriptase promoter mutation, or combined chromosome 7 gain and chromosome 10 loss (1-3). It is noteworthy that incorporating these molecular criteria into the diagnostic framework has substantially improved the precision and biological relevance of diffuse glioma classification (2, 3).

Median survival for patients with GBM remains approximately 15 months (4), an outcome that has improved only modestly despite decades of clinical research, underscoring the biological complexity of the disease. A major challenge is its pronounced heterogeneity: GBM extensively varies within individual tumors and across patients (5-7). Generally, genetic, epigenetic, transcriptional, and cellular differences contribute to treatment resistance, early recurrence, and poor survival (5-8).

Projects such as The Cancer Genome Atlas (TCGA) have remarkably advanced the molecular characterization of GBM by revealing the extent of transcriptional alterations associated with tumor initiation and progression (9). Transcriptomic profiling has become a widely used approach for identifying differentially expressed genes

© 2026 The Author(s); Published by Shahrekord University of Medical Sciences. This is an open-access article distributed under the terms of the Creative Commons Attribution License (https://creativecommons.org/licenses/by/4.0), which permits unrestricted use, distribution, and reproduction in any medium, provided the original work is properly cited.

(DEGs) and the pathways and networks they participate in. In parallel, bioinformatics pipelines now enable systematic interrogation of this complexity in order to prioritize genes with potential biomarker or therapeutic relevance (10).

Two analytical strategies are particularly useful in this context. Gene ontology (GO) and Kyoto Encyclopedia of Genes and Genomes (KEGG) enrichment analyses translate lists of dysregulated genes into biologically interpretable processes and signaling pathways (10). Gene-pathway network analysis can further reveal how candidate genes are distributed across enriched pathways and help prioritize genes with broader pathway involvement for subsequent investigation (11).

In the present study, an integrative bioinformatics framework is applied to GBM transcriptomic data. First, DEGs are identified and then subjected to GO and KEGG functional enrichment analyses, followed by construction of a circular gene–pathway membership network to characterize regulatory modules and prioritize candidate genes associated with disease progression. Rather than simply cataloging dysregulated genes, the primary objective is to identify biologically meaningful pathways and a refined set of candidate genes for future experimental validation. Although several studies have reported transcriptomic alterations in GBM, many have primarily focused on DEG identification without integrating neuronal identity loss, pathway-level enrichment, and candidate gene–pathway connectivity within a single analytical workflow. Therefore, this study seeks to characterize the dominant transcriptional programs altered in GBM and to prioritize cell cycle-related candidate genes for future validation.

Materials and Methods

Data Source and Cohort Definition

Ribonucleic acid-sequencing (RNA-seq) transcriptomic data for GBM were obtained from the TCGA GBM Multiforme (TCGA-GBM) cohort using the TCGAbiolinks package (version 2.40.0) in R software (version 4.x). The dataset comprised 156 primary GBM tumor samples and 5 samples annotated as solid tissue normal. Gene expression data were retrieved in STAR-Counts format and then processed within the R statistical environment.

In addition, raw count data were normalized using the trimmed mean of M values method implemented in the edgeR package (version 4.10.5) in order to account for differences in library size and composition among the samples. Before downstream analyses, lowly expressed genes were filtered out by excluding genes with counts per million values below 10 in at least 70% of samples. The remaining genes were subsequently transformed to the log2 scale, generating a normalized expression matrix suitable for differential expression analysis and downstream bioinformatics investigations.

Moreover, the processed expression matrix was used for differential expression analysis, functional enrichment analysis, gene–pathway network construction, and candidate gene prioritization. Given that all data were obtained from publicly available, de-identified TCGA resources, no additional institutional ethics approval was required for the computational analyses.

The imbalance between tumor and normal samples reflects the composition of the publicly available TCGA-GBM cohort, in which normal brain tissue is inherently limited because healthy brain samples are rarely available for research. Differential expression analysis was conducted using the edgeR package (version 4.10.5) with trimmed mean of M normalization, a widely accepted approach that accommodates unequal group sizes through empirical Bayes estimation of dispersion. This limitation, which is acknowledged in the Discussion section, was considered when interpreting the results.

Transcriptomic Data Acquisition and Preprocessing

Following data retrieval, preprocessing was performed in R software (version 4.x) to prepare the expression matrix for differential expression analysis. Genes with zero or near-zero expression were removed to reduce background noise. After filtering, 10,118 genes were retained in the normalized expression matrix for downstream analyses.

Differential Expression Analysis

Thresholds of absolute log2 fold change ($|\log2FC| > 0.5$ and Benjamini–Hochberg adjusted $P < 0.05$ were applied to identify DEGs between GBM and control samples. Overall, 7,469 DEGs met these criteria and were classified as upregulated or downregulated according to the direction of log2FC.

All statistical analyses were performed in R (version 4.x), with base R functions used for data handling.

Construction of Differentially Expressed Gene Dataset

From the DEG output, a structured dataset containing gene identifiers, log2 fold-change values, statistical significance values, and gene symbols was constructed in R software (version 4.x); this dataset served as the basis for downstream visualization and analysis. Following differential expression analysis, 7,469 genes met the predefined statistical criteria ($|\log2FC| > 0.5$ and adjusted $P < 0.05$). Subsequently, a focused 142-gene panel was employed as the input for GO enrichment analysis, KEGG pathway analysis, and gene-pathway membership network construction.

Data Visualization and Heatmap Construction

The top 50 DEGs by absolute log2 fold change were visualized as a single-column heatmap of scaled log2FC values using the pheatmap package in R software (version 4.x). Each row represents one gene; genes were ordered by the hierarchical clustering of their log2FC values, grouping genes with similar expression shift magnitudes and directions. This visualization reflects gene-level expression shifts in GBM relative to control tissue rather than the clustering of individual samples.

Functional Enrichment Analysis (Kyoto Encyclopedia of Genes and Genomes and Gene Ontology)

To place the 142-gene set in a biological context, KEGG

pathway enrichment analysis was performed using precompiled pathway annotations. Pathways were ranked by adjusted *P* value and combined enrichment score. A total of 159 KEGG pathways were returned, with cell cycle, focal adhesion, spliceosome, cellular senescence, and nitrogen metabolism among the most prominent.

GO biological process enrichment was separately analyzed using the clusterProfiler package after gene symbols were converted to Entrez IDs with org. Hs.eg.db. The analysis showed strong enrichment for mitotic cell-cycle progression, nuclear division regulation, and cell proliferation, along with a smaller group of terms related to membrane organization and wound healing.

Gene-Pathway Membership Network Construction and Candidate Prioritization

To visualize the functional distribution of the selected genes across KEGG pathways, a gene–pathway membership network was constructed using the *circlize* package in R software (version 4.x). The network was generated by mapping genes from the 142-gene set to the KEGG pathways in which they were annotated. Each gene and pathway was represented as a node, and an edge was drawn when a gene was annotated as a member of the corresponding pathway. Thus, the edges indicate pathway co-membership and should not be interpreted as physical protein–protein interactions (PPI), regulatory relationships, or experimentally validated molecular associations.

Cell cycle and focal adhesion, the two pathways that remained statistically significant after Benjamini–Hochberg correction, were treated as the primary inferential findings. Cellular senescence and spliceosome were included only as exploratory pathways because they displayed nominal enrichment but did not satisfy the adjusted *P* value threshold. Therefore, their network connections were descriptively interpreted and were not considered statistically confirmed pathway associations.

Candidate genes were prioritized according to three predefined criteria: (i) significant differential expression in GBM versus normal tissue, defined as $|\log2FC| > 0.5$ and adjusted $P < 0.05$; (ii) membership in at least one enriched KEGG pathway included in the network; and (iii) biological relevance to the dominant statistically significant pathways, particularly cell cycle. Moreover, the number of pathway memberships for each gene was counted descriptively. It should be noted that no PPI analysis, weighted-edge modeling, degree-centrality testing, or formal hub-detection algorithm was performed in this study. Accordingly, the term "candidate gene" is used throughout the manuscript instead of "hub" gene.

Workflow Visualization

A workflow diagram was generated using the DiagrammeR package in R software (version 4.x) in order to summarize the analytical pipeline from data preprocessing and differential expression analysis through gene selection, GO/KEGG enrichment, gene–pathway network construction, and candidate gene identification.

Statistical Analysis and Software Environment

All analyses were conducted in R software (version 4.x). Differential expression was defined by $|\log2FC| > 0.5$ with Benjamini–Hochberg adjusted $P < 0.05$ for multiple-testing correction. Furthermore, downstream enrichment analyses relied on established R packages and publicly available biological databases. Ultimately, data were processed by edgeR and limma, and figures were produced using ggplot2, pheatmap, clusterProfiler, circlize, and DiagrammeR.

Results

Predominant Downregulation of Genes in Glioblastoma

In general, 7,469 DEGs were identified in GBM relative to control samples. Of these, 4,789 genes (64.1%) were downregulated, and 2,680 (35.9%) were upregulated, indicating a clear predominance of transcriptional downregulation.

Distinct Clustering Pattern of Top Differentially Expressed Genes

To visualize the magnitude and direction of expression change across the most dysregulated genes, the top 50 DEGs by absolute log2 fold change were displayed as a single-column heatmap of scaled log2FC values, with genes ordered by hierarchical clustering (Figure 1). Each row represents one gene; in addition, color intensity reflects the log2FC in GBM relative to control tissue, with red depicting upregulation and blue showing downregulation. This approach visualizes gene-level expression shifts rather than sample-level clustering. TOP2*A* (log2FC = 5.79), *LTF* (+ 5.37), and *IGFBP2* (+ 5.32) genes formed a distinct upregulated cluster at the top of the figure, while the remaining 47 genes displayed negative log2FC values and were grouped into a large downregulated block (log2FC range: -5.22 to -6.76). The most strongly downregulated genes included *GRIN1* (log2FC = -6.76), *SLC17A7* (-6.58), *SV2B* (-6.33), *PACSIN1* (-6.24), and *PRKCG* (-6.08), all well-established mediators of synaptic transmission and neuronal function (Table 1). Moreover, the downregulated cluster as a whole was dominated by genes associated with synaptic and neuronal identity, including *GABRA1*, *GABRA5*, *GABRB2*, *GABRG2*, *CACNA1B*, *SNAP25*, *SYT1*, *NEFL*, *NEFM*, and *CAMK2A*, consistent with large-scale loss of neuronal gene expression in GBM tissue.

Likewise, the larger downregulated cluster was strongly enriched for genes involved in synaptic transmission and neuronal identity, including glutamate and gamma-aminobutyric acid (GABA) receptor subunits (*GRIN1*, *GRIN2B*, *GABRA1*, *GABRA5*, *GABRB2*, and *GABRG2*) and voltage-gated calcium-channel components (*CACNA1B* and *CACNG3*). Other associated genes were synaptic vesicle and exocytosis machinery (*SNAP25*, *SYT1*, *SV2B*, *SYN2*, and *CPLX2*) and additional neuron-associated genes (*RBFOX1*, *MYT1L*, *NEFL*, *NEFM*, *CAMK2A*, and *PRKCG*). Collectively, this pattern is consistent with a broad reduction in neuronal and synaptic gene

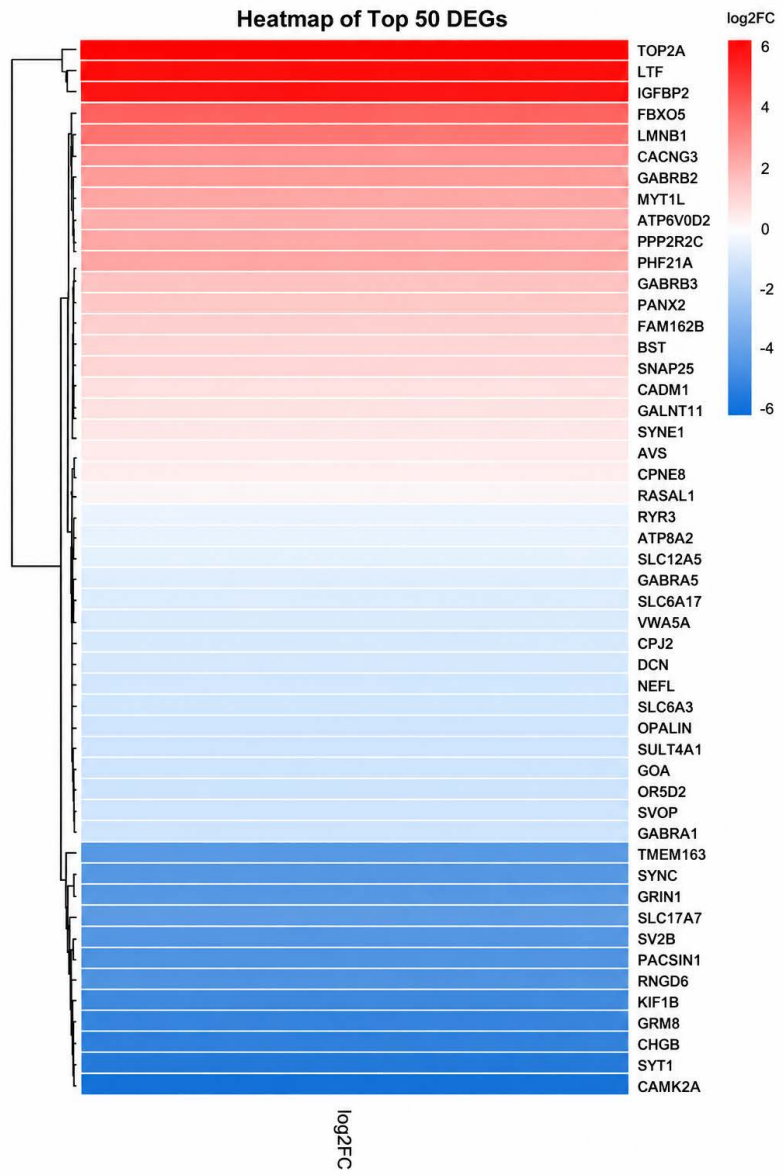

Figure 1. Single-Column Heatmap of Top 50 DEGs

Note. GBM: Glioblastoma: DEGs: Differentially expressed genes. The figure visualizes the 50 most DEGs in GBM, ranked by absolute log2 fold change and displayed as a single-column heatmap of scaled log2FC values (one row per gene). Color intensity reflects the direction and magnitude of expression change in GBM relative to normal brain tissue (red = upregulated; blue = downregulated); further, genes are ordered by the hierarchical clustering of their log2FC values. This figure also shows gene-level expression shifts rather than clustering across individual samples. *TOP2A* (log2FC = 5.79), *LTF* (+5.37), and *IGFBP2* (+5.32) form a distinct upregulated cluster at the top; the remaining 47 genes cluster as a single downregulated block (log2FC −5.22 to −6.76), predominantly comprising neuronal and synaptic markers, including *GRIN1*, *SLC17A7*, *SNAP25*, and *CAMK2A*.

expression as tumor tissue replaces normal neural tissue. In contrast, the three markedly upregulated genes were associated with proliferative and tumor-related functions. *TOP2A* (log2FC = 5.79), the most strongly upregulated gene in the dataset, encodes a topoisomerase involved in DNA replication and is widely recognized as a marker of proliferation in high-grade glioma. In addition, LTF (log2FC = 5.37) encodes lactotransferrin, a multifunctional glycoprotein involved in immune modulation and cell growth, whereas *IGFBP2* (log2FC = 5.32) has repeatedly been related to glioma grade and invasiveness. The coordinated upregulation of these genes is therefore in line with an actively proliferating tumor that is remodeling its microenvironment and infiltrating surrounding brain tissue.

Significant Enrichment of Cell Cycle and Proliferation-Related Pathways

KEGG analysis of the 142-gene set returned 159 associated pathways. Using an adjusted $P < 0.05$ significance threshold, two pathways remained significant: cell cycle ($P = 1.31 \times 10^{-4}$, adjusted $P = 0.0209$) and focal adhesion (adjusted $P = 0.0443$). These pathways therefore represent the statistically supported KEGG findings of this analysis. Additional pathways, including spliceosome, cellular senescence, amoebiasis, progesterone-mediated oocyte maturation, TGF-beta signaling, cytoskeleton in muscle cells, and coronavirus disease 2019, demonstrated nominal enrichment but did not remain significant after multiple-testing correction and were reported for descriptive purposes only. When pathways were ranked by combined enrichment score irrespective of statistical significance,

nitrogen metabolism had the highest score (approximately 96), followed by cell cycle (approximately 61) and focal adhesion (approximately 40), respectively (Figure 2). Thus, cell cycle and focal adhesion were the only KEGG pathways supported by the adjusted significance threshold.

Cell Cycle-Associated Candidate Genes Identified Through Gene–Pathway Network Membership Analysis

The circular gene–pathway interaction network revealed a highly concentrated connectivity pattern, with the cell cycle pathway accounting for the majority of gene–pathway associations (Figure 3). Furthermore, genes were arranged around the outer arc, with lines indicating their membership in enriched pathways. Red and grey connections represented upregulated and downregulated genes, respectively.

Table 1. Top DEGs in GBM Compared to Normal Brain Tissue

Gene	Log2 Fold Change	Regulation
GRIN1	-6.758	Down
SLC17A7	-6.583	Down
SV2B	-6.328	Down
PACSIN1	-6.244	Down
PRKCG	-6.082	Down
CHD5	-5.982	Down
SNAP25	-5.278	Down
ATP2B3	-5.252	Down
PPP2R2C	-5.226	Down
PHF24	-5.225	Down
GABRB2	-5.221	Down
RAB3C	-5.219	Down
TOP2A	5.785	Up
IGFBP2	5.325	Up
LTF	5.375	Up

Note. GBM: Glioblastoma: DEGs: Differentially expressed genes.

Among the upregulated genes, *CCNB1*, *CDC20*, *CCNA2*, *MYC*, *BUB1*, *WEE1*, and *E2F5* were prioritized because they were significantly differentially expressed and annotated to the statistically significant cell cycle pathway (Table 2). In addition, *CCNA2*, *CCNB1*, *MYC*, and *E2F5* were annotated to the nominally enriched cellular senescence pathway. Considering that cellular senescence did not remain significant after multiple-testing correction, these associations were interpreted as exploratory rather than statistically confirmed evidence of pathway overlap. Additional cell cycle-associated genes included *AURKA*, *CDCA8*, *SKP2*, *KIF20A*, *DLGAP5*, *TROAP*, and *RCC1*, reflecting the broad activation of mitotic processes in GBM. Moreover, downregulated genes, including *PDGFRB*, *VCL*, *SOX9*, *SPARC*, *TIMP3*, and *TNFRSF1A*, were primarily related to the focal adhesion and cellular senescence pathways.

Likewise, several genes were connected to more than one pathway, reflecting shared functional annotations within the KEGG database rather than direct regulatory interactions. In particular, the co-membership of *CCNA2*, *CCNB1*, *MYC*, and *E2F5* in the cell cycle and cellular senescence pathways is consistent with their established roles in proliferation and senescence-related processes and should not be interpreted as a novel or GBM-specific regulatory relationship. Similarly, *PDGFRB*, *VCL*, and *CAV1* were associated with the focal adhesion pathway, while *HNRNPA1* and *SRSF3* were linked to the spliceosome pathway.

Overall, the network demonstrated that GBM-associated transcriptional alterations converge on a limited number of core biological pathways rather than being broadly distributed across multiple processes. Importantly, this network represents gene–pathway membership rather than physical PPIs. Further, the prioritized candidate genes

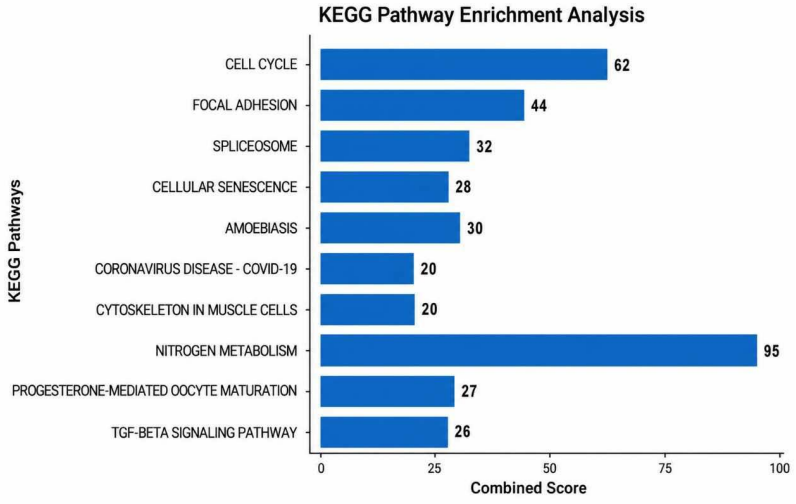

Figure 2. KEGG Pathway Enrichment Analysis: Top 10 Pathways for the 142-Gene Set, Ranked by Combined Enrichment Score
Note. KEGG: Kyoto Encyclopedia of Genes and Genomes; TGF: Transforming growth factor; COVID-19: Coronavirus disease 2019. Nitrogen metabolism achieved the highest combined score (≈96), followed by cell cycle (≈61) and focal adhesion (≈40). The remaining top-ranked pathways included spliceosome, amoebiasis, cellular senescence, progesterone-mediated oocyte maturation, TGF-beta signaling, cytoskeleton in muscle cells, and coronavirus disease COVID-19. Cell cycle ranked first when pathways were instead ordered by adjusted *P* value (adjusted $P = 0.0209$), highlighting the complementary information provided by the two ranking metrics.

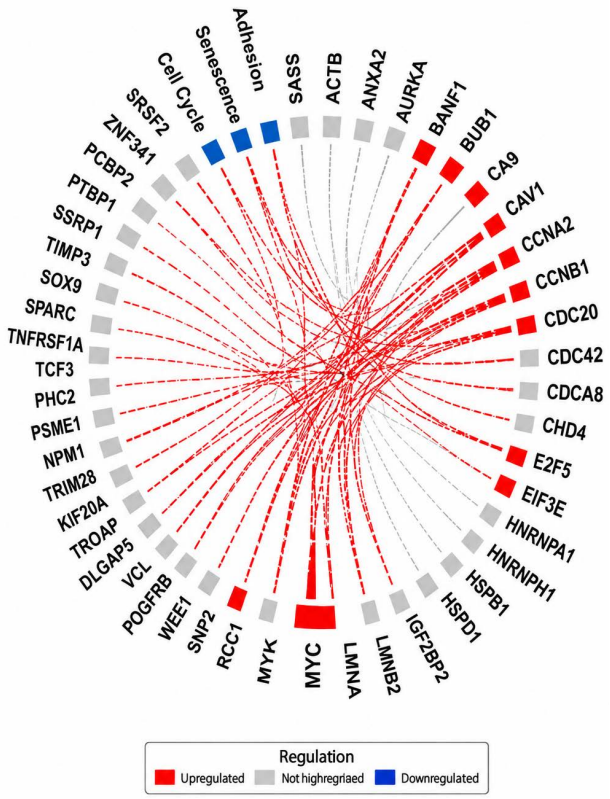

Figure 3. Gene-Pathway Membership Network

Note. KEGG: Kyoto Encyclopedia of Genes and Genomes; DEG: Differentially expressed gene. Circular visualization generated using the *circlize* package in R software, showing the membership of DEGs in selected KEGG pathways. Each line represents the annotation of a gene to a pathway and does not indicate a physical protein-protein interaction or a direct regulatory relationship. Cell cycle and focal adhesion were statistically significant after multiple-testing correction, whereas cellular senescence and spliceosome were retained as exploratory pathways based on nominal enrichment. Red gene sectors display upregulated genes, whereas grey sectors depict downregulated genes. The network was used for descriptive functional interpretation and candidate prioritization rather than formal hub detection.

were selected based on significant differential expression together with pathway annotation.

Enrichment of Cell Cycle and Mitotic Biological Processes

GO biological process analysis reinforced the cell-cycle pattern observed in the KEGG results (Figure 4). Based on the results, mitotic cell-cycle phase transition ranked highest by both gene count (15 genes) and statistical significance, followed by mitotic nuclear division and positive regulation of the cell cycle (11 genes each), positive regulation of cell-cycle processes (10 genes), and regulation of mitotic/nuclear division (9 genes each). In addition, the top terms included wound healing (12 genes), membrane assembly, membrane biogenesis, and collagen fibril organization (6 genes each), suggesting a secondary pattern of extracellular-matrix remodeling and tissue-repair-like activity alongside the dominant proliferative signal. This combined pattern is consistent with the highly proliferative and invasive biology of GBM.

Differential expression analysis, selection of the 142-gene set, functional enrichment analyses (GO and KEGG), and gene–pathway network construction were integrated into a systematic analytical framework. This stepwise pipeline provided a structured transition from transcriptomic data to biologically interpretable findings, ultimately prioritizing *WEE1*, *CCNB1*, *CDC20*, *BUB1*, *CCNA2*, *MYC*, and *E2F5* genes as key cell cycle-associated candidates for further investigation (Figure 5). The workflow illustrates how sequential filtering and functional annotation can reduce analytical complexity while retaining biologically relevant signals associated with GBM pathogenesis.

Table 2. Key Cell Cycle-Associated Candidate Genes Identified in GBM Through Gene-Pathway Network Analysis

Gene	Log2 Fold Change	Regulation	Associated Pathway(s)
BUB1	3.746	Up	Cell cycle
CDC20	3.445	Up	Cell cycle
CCNA2	3.166	Up	Cell cycle and cellular senescence
WEE1	3.121	Up	Cell cycle
CCNB1	2.574	Up	Cell cycle and cellular senescence
MYC	2.061	Up	Cell cycle and cellular senescence
E2F5	1.487247	Up	Cell cycle and cellular senescence

Note. GBM: Glioblastoma.

Discussion

GBM exhibited extensive and markedly asymmetric transcriptional dysregulation, with substantially more downregulated than upregulated genes. The most strongly downregulated genes were predominantly associated with neuronal and synaptic functions, whereas a small group of highly upregulated genes, including *TOP2A*, *LTF*, and *IGFBP2*, was related to proliferation, tumor progression, and microenvironmental remodeling. This pattern conforms to the profound molecular heterogeneity and transcriptional reprogramming characteristic of GBM (5-8). However, given that the present analysis was based on bulk transcriptomic data, the widespread reduction in neuronal gene expression may partly reflect differences in tissue composition and tumor purity rather than exclusively tumor-cell-intrinsic transcriptional repression.

The coordinated downregulation of genes involved in glutamatergic and GABAergic signaling, synaptic vesicle function, ion-channel activity, and neuronal structural integrity suggest a broad loss of normal neuronal transcriptional identity. In contrast, the marked upregulation of *TOP2A* and *IGFBP2* is biologically consistent with the highly proliferative and invasive phenotype of GBM (12). Overall, these findings indicate that GBM-associated transcriptional remodeling involves the activation of tumor-promoting programs and the suppression of normal neural functions.

Functional enrichment analyses further supported this interpretation. Cell cycle was the most statistically significant KEGG pathway, while focal adhesion was the only other pathway that remained significant after multiple-testing correction. These findings corroborate two major biological features of GBM: uncontrolled proliferation and invasive interaction with the surrounding extracellular matrix (4, 6). Other pathways, including

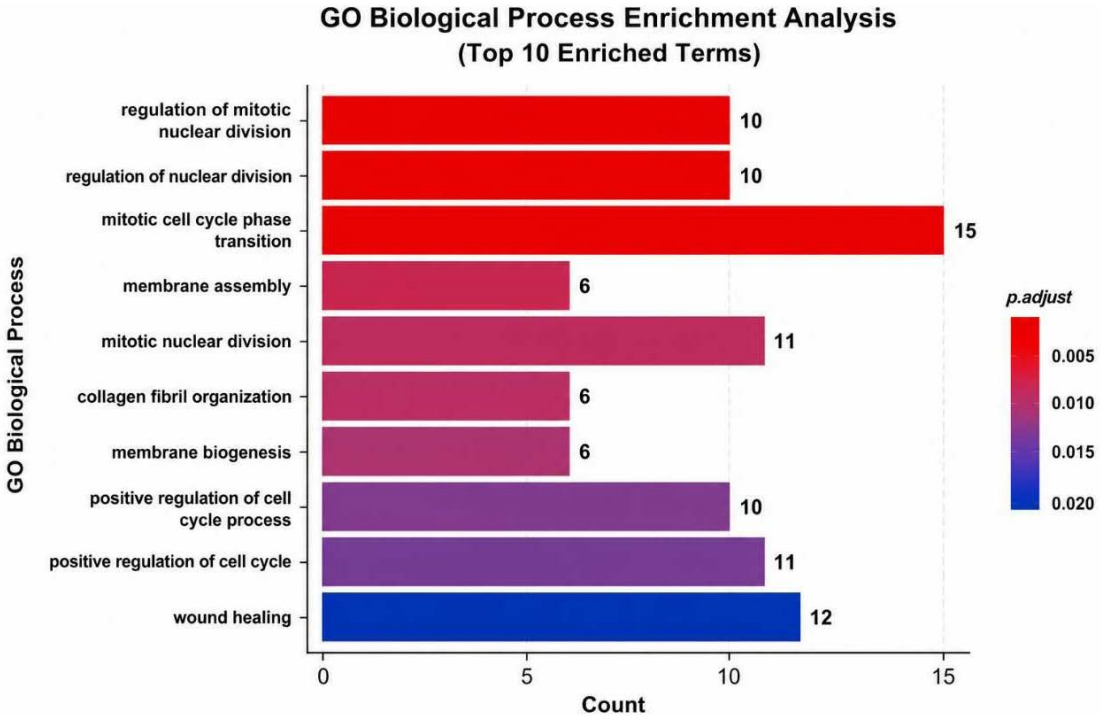

Figure 4. GO Biological Process Enrichment: Top 10 GO Biological Process Terms for the 142-Gene Set
Note. GO: Gene ontology. Color encodes adjusted *P* value (red = most significant, blue = least significant). Mitotic cell cycle phase transition ranks first in both gene count (15 genes) and statistical significance, followed by mitotic nuclear division and positive regulation of cell cycle (11 genes each), positive regulation of cell cycle process (10), and regulation of mitotic/nuclear division (9 each). Moreover, wound healing (12 genes), membrane assembly, membrane biogenesis, and collagen fibril organization (6 genes each) appear, pointing to a secondary extracellular matrix remodeling signature alongside the dominant proliferative theme.

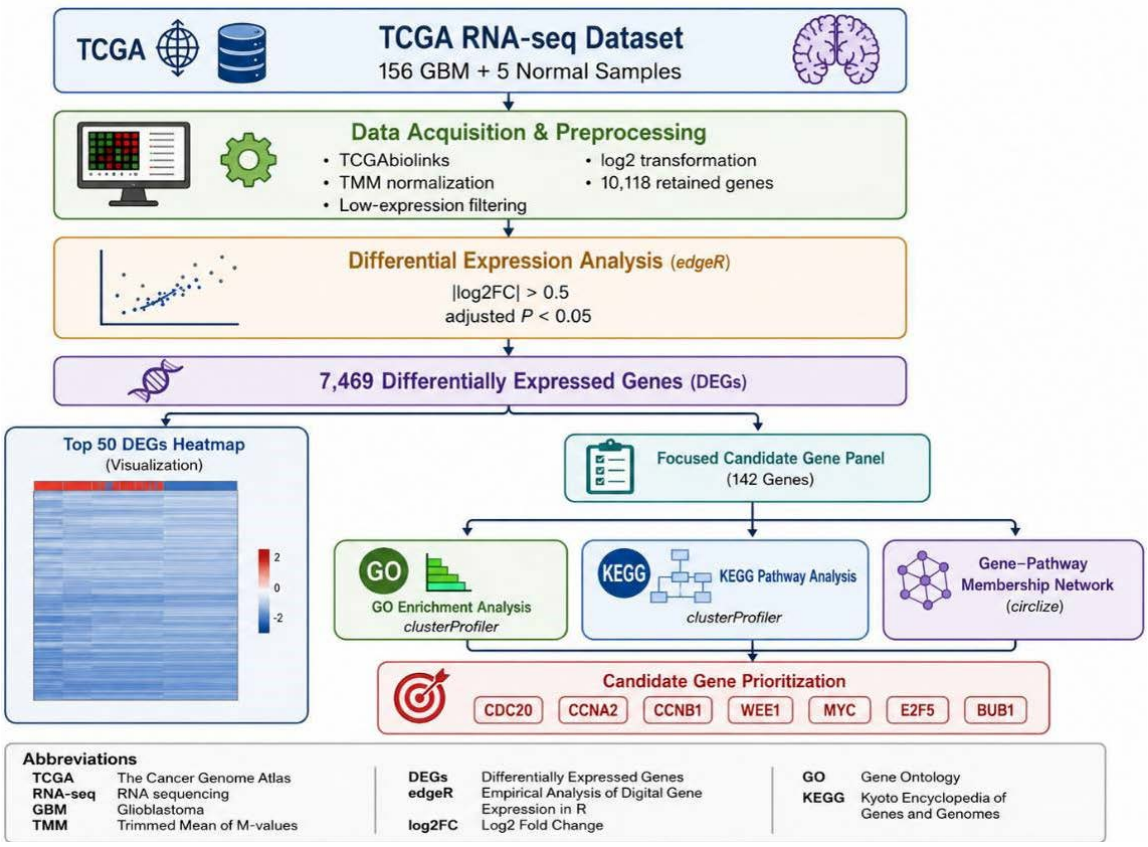

Figure 5. Bioinformatics Workflow of the Present Study
Note. TCGA: The Cancer Genome Atlas; GBM: Glioblastoma; RNA-seq: Ribonucleic acid sequencing; DEG: Differentially expressed gene; KEGG: Kyoto Encyclopedia of Genes and Genomes; GO: Gene ontology. RNA-seq expression profiles of 156 GBM and 5 normal brain samples were obtained from TCGA. Following data acquisition and preprocessing, differential expression analysis was performed using the edgeR package with thresholds of $|\log_2 FC| > 0.5$ and adjusted $P < 0.05$, resulting in 7,469 DEGs. Further, the top 50 DEGs were visualized as a heatmap, while a focused candidate gene panel comprising 142 genes was subsequently used for downstream GO enrichment analysis, KEGG pathway analysis, and construction of a gene–pathway membership network using the *circlize* package. Finally, the integrated analyses enabled the prioritization of candidate genes associated with the molecular mechanisms underlying GBM.

cellular senescence, spliceosome, and nitrogen metabolism, demonstrated descriptive enrichment but did not remain significant after correction; therefore, they should be considered exploratory rather than confirmed findings. Similarly, GO analysis emphasized mitotic cell-cycle progression and nuclear division, whereas enrichment of wound healing, membrane organization, and collagen-related processes represented an additional contribution of extracellular matrix remodeling to GBM biology.

The gene-pathway membership network prioritized *CDC20*, *CCNA2*, *CCNB1*, *WEE1*, *MYC*, *E2F5*, and *BUB1* as cell cycle-associated candidate genes. Their biological functions are in conformity with the dominant proliferative signature identified in this study. *WEE1* regulates the G2/M checkpoint and has been investigated as a therapeutic target in several cancers, including GBM (13). In addition, *CDC20*, *CCNB1*, *BUB1*, and *CCNA2* participate in mitotic progression and checkpoint regulation and have been associated with aggressive tumor behavior and unfavorable clinical outcomes (14-17). Likewise, *MYC* contributes to GBM cell renewal and metabolic reprogramming (18). Accordingly, the convergence of these genes within the cell cycle pathway supports their prioritization for future functional validation.

Likewise, several candidates, including *CCNA2*, *CCNB1*, *MYC*, and *E2F5*, were annotated to the cellular senescence pathway. Although this pathway did not remain statistically significant after multiple-testing correction, the overlap is biologically plausible given the close relationship between cell-cycle regulation and cellular senescence. Recent evidence suggests that senescent malignant cells may contribute to GBM progression and treatment resistance (19). Nevertheless, these associations should be regarded as exploratory because the present analysis demonstrates pathway co-membership rather than direct regulatory interactions.

Importantly, the gene-pathway network used in this study should not be interpreted as a PPI network. The identified connections demonstrated shared KEGG pathway annotations, and the prioritized genes were selected based on significant differential expression and biological relevance to enriched pathways. Accordingly, *CDC20*, *CCNA2*, *CCNB1*, *WEE1*, *MYC*, *E2F5*, and *BUB1* should be considered candidate genes rather than formally established hub genes. Confirmation of hub status would require complementary approaches such as PPI analysis or weighted gene co-expression network analysis.

Moreover, the neuronal/synaptic transcriptional signature identified in this study may have potential biological and clinical relevance. Coordinated suppression of neuronal genes could provide a useful molecular representation of the loss of normal neural identity accompanying tumor infiltration and progression. However, the present study did not establish diagnostic or prognostic utility, and independent clinical validation would be required before these transcriptional patterns could be considered for patient stratification or therapeutic monitoring.

Several limitations should be taken into consideration. First, despite vast computational analysis, and the prioritized candidate genes require experimental validation to establish their functional roles in GBM. Further, the network depends on existing KEGG pathway annotations and therefore cannot demonstrate direct molecular interactions or causal relationships. In addition, the TCGA-GBM cohort contains substantially fewer normal than tumor samples, reflecting the limited availability of normal brain tissue. Although the statistical approach accommodates unequal group sizes, validation in independent datasets containing larger numbers of normal samples would strengthen the findings. Finally, prospective cohorts with clinical outcome data will be required to determine whether the identified candidate genes have prognostic or therapeutic value.

Conclusion

This analysis characterized GBM as a disease marked by extensive and asymmetric transcriptional dysregulation, with a small group of strongly upregulated proliferation-associated and invasion-associated genes (*TOP2A*, *LTF*, and *IGFBP2*) contrasted by broad downregulation of neuronal and synaptic genes. Among the statistically significant KEGG findings, cell cycle and focal adhesion showed the strongest evidence of enrichment. The gene–pathway membership network also prioritized seven upregulated candidate genes (*CDC20*, *CCNA2*, *CCNB1*, *WEE1*, *MYC*, *E2F5*, and *BUB1*), all of which were associated with cell-cycle control, with several also annotated to cellular senescence. These candidates were prioritized based on differential expression and pathway membership; future studies incorporating PPI or co-expression analyses are required to formally assess hub status. Collectively, these findings reinforce cell-cycle dysregulation as a central feature of GBM pathogenesis, providing a focused set of biologically coherent candidates for experimental validation.

Acknowledgments

The authors would like to thank the TCGA Research Network for providing access to the publicly available transcriptomic data used in this study.

Artificial Intelligence Use Disclosure

During the preparation of this manuscript, the authors used Claude (Anthropic) for language editing and formatting assistance. In addition, artificial intelligence–assisted tools were employed to design and visually refine the bioinformatics workflow figure (Figure 5). All scientific content, data interpretation, and final figure elements were reviewed and verified by the authors.

Authors' Contribution

Conceptualization: Maryam Peymani
Data Curation: Elaheh Maherani and Maryam Peymani
Formal Analysis: Elaheh Maherani
Investigation: Elaheh Maherani and Maryam Peymani
Methodology: Maryam Peymani
Project Administration: Maryam Peymani
Resources: Maryam Peymani
Software: Elaheh Maherani
Supervision: Maryam Peymani and Samira Asgharzade
Validation: Samira Asgharzade, Ali Zarrabi, and Fatemeh Azizi

Farsani
Visualization: Elaheh Maherani
Writing–Original Draft: Elaheh Maherani and Maryam Peymani
Writing–Review and Editing: Maryam Peymani, Samira Asgharzade, and Ali Zarrabi

Competing Interests
The authors declare that they have no competing interests.

Data Availability Statement
The datasets analyzed during this study are publicly available in TCGA via the Genomic Data Commons Data Portal.

Ethical Approval
The study was approved by the Ethics Committee of Islamic Azad University, Shahrekord Branch, Shahrekord, Iran (approval code: IR.IAU.SHK.REC.1405.052).

Funding
This research received no specific grant from any funding agency in the public, commercial, or not-for-profit sectors.

References
1. Louis DN, Perry A, Wesseling P, Brat DJ, Cree IA, Figarella-Branger D, et al. The 2021 WHO classification of tumors of the central nervous system: a summary. Neuro Oncol 2021;23(8):1231-51. doi:10.1093/neuonc/noab106
2. Horbinski C, Berger T, Packer RJ, Wen PY. Clinical implications of the 2021 edition of the WHO classification of central nervous system tumours. Nat Rev Neurol 2022;18(9):515-29. doi:10.1038/s41582-022-00679-w
3. Komori T. Grading of adult diffuse gliomas according to the 2021 WHO classification of tumors of the central nervous system. Lab Invest 2022;102(2):126-33. doi:10.1038/s41374-021-00667-6
4. Khabibov M, Garifullin A, Boumber Y, Khaddour K, Fernandez M, Khamitov F, et al. Signaling pathways and therapeutic approaches in glioblastoma multiforme (review). Int J Oncol 2022;60(6):69. doi:10.3892/ijo.2022.5359
5. Eisenbarth D, Wang YA. Glioblastoma heterogeneity at single cell resolution. Oncogene 2023;42(27):2155-65. doi:10.1038/s41388-023-02738-y
6. Rabah N, Ait Mohand FE, Kravchenko-Balasha N. Understanding glioblastoma signaling, heterogeneity, invasiveness, and drug delivery barriers. Int J Mol Sci 2023;24(18):14256. doi:10.3390/ijms241814256
7. Lauko A, Lo A, Ahluwalia MS, Lathia JD. Cancer cell heterogeneity & plasticity in glioblastoma and brain tumors. Semin Cancer Biol 2022;82:162-75. doi:10.1016/j.semcancer.2021.02.014
8. Pombo Antunes AR, Scheyltjens I, Lodi F, Messiaen J, Antoranz A, Duerinck J, et al. Single-cell profiling of myeloid cells in glioblastoma across species and disease stage reveals macrophage competition and specialization. Nat Neurosci 2021;24(4):595-610. doi:10.1038/s41593-020-00789-y
9. Zakharova G, Efimov V, Raevskiy M, Rumiantsev P, Gudkov A, Belogurova-Ovchinnikova O, et al. Reclassification of TCGA diffuse glioma profiles linked to transcriptomic, epigenetic, genomic and clinical data, according to the 2021 WHO CNS tumor classification. Int J Mol Sci 2022;24(1):157. doi:10.3390/ijms24010157
10. Wu T, Hu E, Xu S, Chen M, Guo P, Dai Z, et al. clusterProfiler 4.0: a universal enrichment tool for interpreting omics data. Innovation (Camb) 2021;2(3):100141. doi:10.1016/j.xinn.2021.100141
11. Xu S, Hu E, Cai Y, Xie Z, Luo X, Zhan L, et al. Using clusterProfiler to characterize multiomics data. Nat Protoc 2024;19(11):3292-320. doi:10.1038/s41596-024-01020-z
12. Tang J, Karbhari N, Campian JL. Therapeutic targets in glioblastoma: molecular pathways, emerging strategies, and future directions. Cells 2025;14(7):494. doi:10.3390/cells14070494
13. Wang Z, Li W, Li F, Xiao R. An update of predictive biomarkers related to WEE1 inhibition in cancer therapy. J Cancer Res Clin Oncol 2024;150(1):13. doi:10.1007/s00432-023-05527-y
14. Zhou R, Zhang K, Dai T, Guo Z, Li T, Hong X. Construction and validation of cell cycle-related prognostic genetic model for glioblastoma. Medicine (Baltimore) 2024;103(40): e39205. doi:10.1097/md.0000000000039205
15. Zhong J, Shi S, Peng W, Cui H, Sun X. HMGN2 accelerates the proliferation and cell cycle progression of glioblastoma by regulating CDC20 expression. Genes Dis 2025;12(3):101433. doi:10.1016/j.gendis.2024.101433
16. Cicirò Y, Ragusa D, Sala A. Expression of the checkpoint kinase BUB1 is a predictor of response to cancer therapies. Sci Rep 2024;14(1):4461. doi:10.1038/s41598-024-55080-y
17. Zhou HY, Wang YC, Wang T, Wu W, Cao YY, Zhang BC, et al. CCNA2 and NEK2 regulate glioblastoma progression by targeting the cell cycle. Oncol Lett 2024;27(5):206. doi:10.3892/ol.2024.14339
18. Duan Y, Liu Z, Wang Q, Zhang J, Liu J, Zhang Z, et al. Targeting MYC: multidimensional regulation and therapeutic strategies in oncology. Genes Dis 2025;12(4):101435. doi:10.1016/j.gendis.2024.101435
19. Salam R, Saliou A, Bielle F, Bertrand M, Antoniewski C, Carpentier C, et al. Cellular senescence in malignant cells promotes tumor progression in mouse and patient glioblastoma. Nat Commun 2023;14(1):441. doi:10.1038/s41467-023-36124-9